

# An Interval Analysis Based Study for the Design and the Comparison of 3-DOF Parallel Kinematic Machines

D. Chablat<sup>1</sup> Ph. Wenger<sup>1</sup> F. Majou<sup>1</sup> J-P. Merlet<sup>2</sup>

<sup>1</sup>Institut de Recherche en Communications et Cybernétique de Nantes \*

1, rue de la Noë, 44321 Nantes, France

<sup>2</sup>INRIA Sophia-Antipolis

2004 Route des Lucioles, 06902 Sophia Antipolis, France

Damien.Chablat@irccyn.ec-nantes.fr

Philippe.Wenger@irccyn.ec-nantes.fr

Félix.Majou@irccyn.ec-nantes.fr

Jean-Pierre.Merlet@sophia.inria.fr

## Abstract

This paper addresses an interval analysis based study that is applied to the design and the comparison of 3-DOF parallel kinematic machines. Two design criteria are used, (i) a regular workspace shape and, (ii) a kinetostatic performance index that needs to be as homogeneous as possible throughout the workspace. The interval analysis based method takes these two criteria into account: on the basis of prescribed kinetostatic performances, the workspace is analysed to find out the largest regular dextrous workspace enclosed in the Cartesian workspace. An algorithm describing this method is introduced. Two 3-DOF translational parallel mechanisms designed for machining applications are compared using this method. The first machine features three fixed linear joints which are mounted orthogonally and the second one features three linear joints which are mounted in parallel. In both cases, the mobile platform moves in the Cartesian  $x - y - z$  space with fixed orientation.

**Keywords:** Parallel kinematic machine, Design, Interval analysis, Comparison, Workspace, Transmission factors.

---

\*IRCCyN: UMR n° 6597 CNRS, Ecole Centrale de Nantes, Université de Nantes, Ecole des Mines de Nantes

# 1 Introduction

Parallel kinematic machines (PKM) are known for their high dynamic performances and low positioning errors. The kinematic design of PKM has drawn the interest of several researchers. The workspace is usually considered as a relevant design criterion [1, 2, 3]. Parallel singularities [4] occur in the workspace where the moving platform cannot resist any effort. Thus are very undesirable and generally eliminated by design. The Jacobian matrix, which relates the joint rates to the output velocities is generally not constant and not isotropic. Consequently, the performances (e.g. maximum speeds, forces, accuracy and stiffness) vary considerably for different points in the Cartesian workspace and for different directions at one given point. This is a serious drawback for machining applications [5, 6, 7]. Few parallel mechanisms are isotropic throughout the workspace [8, 9]. But their low structural stiffness make them inadequate for machining applications because their legs are subject to bending.

To be of interest for machining applications, a PKM should preserve good workspace properties, that is, regular workspace shape and acceptable kinetostatic performances throughout. For example in milling applications, the machining conditions must remain constant along the whole tool path [10, 11]. In many research papers, this criterion is not taken into account in the algorithmic methods used to compute the workspace volume [12, 13]. Other papers present methods that compute the well-conditioned workspace using discretization [14, 15]. Thus, the results they provide cannot be proved formally. Conversely, interval analysis methods applied to well-conditioned workspace computation provide guaranteed results [16, 17].

The comparison of PKM architectures is a difficult but relevant challenge [7, 18]. Providing tools to allow designers or end-users to rigorously compare PKM is indeed necessary since the variety of existing PKM makes it hard to choose which one is best-suited for a specific task.

In this paper, an interval analysis based method is addressed for the design and comparison of 3-DOF PKM. This method takes into account two criteria, (i) a regular workspace shape and, (ii) a kinetostatic performance index that needs to be as homogeneous as possible throughout the workspace. Two basic tools and an algorithm that considers these two criteria are introduced: on the basis of prescribed kinetostatic performances, the workspace is analyzed to find out the largest regular dextrous workspace (square, cube, cylinder, etc...) enclosed in the Cartesian workspace.

Two translational parallel mechanisms derived from the Delta robot [2] are compared using this method. The first machine, called Orthoglide [19], features three fixed linear joints which are mounted orthogonally and the second one, called UraneSX (Renault Automation) [20], features three linear joints which are mounted in parallel. In both cases, the mobile platform moves in the Cartesian  $x - y - z$  space with fixed orientation.

Next section presents the interval analysis based method for 3-DOF PKM design. Section 3 presents the Orthoglide and UraneSX mechanisms, their kinematic equations and singularity analysis. Section 4 reports the comparison between the two mechanisms through the determination of the largest dextrous cube for the Orthoglide and the largest dextrous square for the UraneSX enclosed in the workspace.

## 2 Description of the interval analysis based method for 3-DOF translational PKM design

### 2.1 Preliminaries

#### 2.1.1 Dextrous Cartesian workspace

For a 3-axis serial machine-tool, a parallelepiped-shaped Cartesian workspace allows the end-user to visualize easily where to place cutting paths. This consideration should also hold for PKM. However the workspace shape is often geometrically complex and thus hard to visualize. Therefore, a regular-shaped workspace is needed for PKM. Thus, we need to define a regular dextrous workspace which is a regular-shaped workspace included in the machine Cartesian workspace. Throughout the dextrous workspace, a kinetostatic performance index (that is chosen beforehand) remains as homogeneous as possible. This index can be the local or global conditioning [3] of the Jacobian matrix  $\mathbf{J}$  (that maps the actuated joint rates of the manipulator into the velocity of the mobile platform), the force or velocity transmission factors. These last two indices make sense for 3-DOF translational PKM with identical actuated joints.

The method presented in this paper aims at designing such 3-DOF PKM. The velocity transmission factors are the ratio between the actuated joints velocities and the velocity of the mobile platform. They are the square roots  $\psi_1$ ,  $\psi_2$  and  $\psi_3$  of the real eigenvalues  $\sigma_1$ ,  $\sigma_2$  and  $\sigma_3$  of  $(\mathbf{J}\mathbf{J}^T)^{-1}$ . In order to keep homogeneous kinetostatic properties, these factors are bounded inside the dextrous workspace. The *regular dextrous Cartesian workspace* can be defined as a set of points  $P$  in the workspace such that  $\psi_1$ ,  $\psi_2$  and  $\psi_3$  are bounded, that is,

$$\mathcal{W}_{Dextrous} = \{P \in \mathcal{W} \mid \psi_{min} \leq \psi_i(P) \leq \psi_{max}, \quad i = 1, 2, 3\} \quad (1)$$

Points  $P$  in  $\mathcal{W}_{Dextrous}$  are called *dextrous points*.

The values of  $\psi_{min}$  and  $\psi_{max}$  (resp.  $\sigma_{min}$  and  $\sigma_{max}$ ) depend on given performance requirements. The method described further aims at computing the largest dextrous Cartesian workspace included in the Cartesian workspace, so that its ratio to the Cartesian workspace is the best one. To be of real interest for milling applications, a PKM must indeed include a large regular dextrous workspace in its Cartesian workspace.

#### 2.1.2 Introduction to ALIAS library

An algorithm for the definition of the largest dextrous workspace included in the Cartesian workspace is described in the following sections. This algorithm uses the ALIAS library [16], which is a C++ library of algorithms based on interval analysis. These algorithms deal with systems of equations and inequalities whose expressions are an arbitrary combination of the most classical mathematical functions (algebraic terms, sine, cosine, log etc..) and whose coefficients are real numbers or, in some cases, intervals. An interface exists with Maple that allows the automatic generation of C++ codes being given the Maple description of the system and then to compile and

run the generated code in order to get the result within the Maple session. Without being exhaustive, **ALIAS** library provides algorithms that enable one to, (i) find an approximation of the real roots of n-dimensional systems, (ii) find an approximation of the variety defined by n-dimensional systems, (iii) find an approximation of the global minimum or maximum of a function (eventually under equations and/or inequalities constraints) up to an accuracy provided by the user, (iv) analyze a system of algebraic equations to determine bounds for its real roots.

### 2.1.3 Geometric constraints

The dextrous workspace  $\mathcal{W}_{Dextrous}$  is defined in Eq. 1 as a function of the eigenvalues of  $(\mathbf{J}\mathbf{J}^T)^{-1}$ . These eigenvalues are determined by solving the third degree characteristic polynomial  $\mathcal{P}$  of  $(\mathbf{J}\mathbf{J}^T)^{-1}$ . To decrease the computing time and to avoid numerical problems on singularities, it is recommended to add geometrical constraints. These constraints naturally depend on the mechanism architecture (see §4.2).

## 2.2 A first basic tool: Box verification

Our purpose is to determine the largest regular dextrous workspace that is enclosed in the Cartesian workspace. For a given point, we note *valid point* if it is a dextrous point and *invalid point* otherwise. For that purpose we need to design first a procedure, called  $\mathcal{M}(B)$ , that takes as input a Cartesian box  $B$  and returns:

- 1: if every point in  $B$  is valid,
- -1: if no point in  $B$  is valid,
- 0: if neither of the other two conditions could be verified.

The first step of this procedure consists in considering an arbitrary point of the box (e.g. its center) and to compute the eigenvalues at this point: either all of them lie in the range  $[\sigma_{min}, \sigma_{max}]$  in which case the center is called *valid* or at least one of them lie outside this range and the center point is denoted *invalid*.

### 2.2.1 Valid center point

In that case if we are able to check that there is no point in  $B$  such that one of the eigenvalues at this point is equal to  $\sigma_{min}$  or  $\sigma_{max}$ , then we can guarantee that every point in  $B$  is valid. Indeed assume that at a given point  $B$  the lowest eigenvalue is lower than  $\sigma_{min}$ : this implies that somewhere along the line joining this point to the center of the box the lowest eigenvalue is exactly  $\sigma_{min}$ .

To perform this check we set the unknown in the characteristic polynomial  $\mathcal{P}$  of  $(\mathbf{J}\mathbf{J}^T)^{-1}$  to  $\sigma_{min}$  (and then to  $\sigma_{max}$ ) and we get a polynomial in  $x, y, z$  only. We now have to determine if there exists some values for these three Cartesian coordinates that cancel the polynomial, being understood that these values have to define a point belonging to  $B$ . This is done by using an interval analysis algorithm from the **ALIAS** library [16]. The principle of this algorithm is to calculate first the polynomial value for the center point  $C_B$  of  $B$ . Without

lack of generality we may assume that this value is positive. If we are able to determine a point  $S_B$  in  $B$  such that the polynomial value at this point is negative, then we can guarantee that there exists a point on the line joining  $C_B$  to  $S_B$  such that the polynomial is exactly 0. The purpose of the algorithm is now to determine if such a point exist. Now let  $B_i$  be a box included in  $B$ : using interval analysis we are able to calculate a range  $[m_{B_i}, M_{B_i}]$  such that for any point  $X$  in  $B_i$  we have  $m_{B_i} \leq \mathcal{P}(X) \leq M_{B_i}$ . Note that this interval evaluation is numerically safe as the bounds of the range are calculated by taking into account round-off errors. On the other hand these bounds may not be *sharp* i.e. there may be no  $X$  in  $B_i$  such that  $\mathcal{P}(X) = m_{B_i}$  or  $M_{B_i}$ . Note, however, that the width of the overestimation decreases with the width of  $B_i$ . Furthermore we may get a sharp evaluation by using, for instance, the derivatives of  $\mathcal{P}$ . Indeed we may calculate the interval evaluation  $[r_{x,y,z}, R_{x,y,z}]$  of  $\partial\mathcal{P}/\partial x, y, z$  and if all three interval evaluations have constant signs (i.e.  $r_{x,y,z} > 0$  or  $R_{x,y,z} < 0$ ), then sharp  $m_{B_i}, M_{B_i}$  are obtained by setting the variables to fixed values. For instance if  $r_x > 0$ , then  $m_{B_i}(M_{B_i})$  is obtained by setting  $x$  to its lower (upper) bound. Note that other methods may also be used to determine sharp bounds (see [21, 22, 23]).

Hence we have the following properties:

1. if  $m_{B_i} > 0$ , then for any point in  $B_i$  the polynomial  $\mathcal{P}$  is positive
2. if  $M_{B_i} < 0$ , then for any point in  $B_i$  the polynomial  $\mathcal{P}$  is negative
3. if  $m_{B_i} < 0$  and  $M_{B_i} > 0$  and the bounds are sharp, then the polynomial  $\mathcal{P}$  cancels in  $B_i$
4. if  $m_{B_i} < 0$  and  $M_{B_i} > 0$  and the bounds are not sharp, then we cannot guarantee the sign of the polynomial  $\mathcal{P}$  within  $B_i$

At that point a simple branch-and-bound algorithm is used: the initial box  $B$  is bisected until either all the sub-boxes resulting from the bisection satisfy property 1 (in which case we can guarantee that the polynomial  $\mathcal{P}$  never cancels for  $B$  and consequently that all the eigenvalues of  $\mathcal{P}$  lie in the range  $[\sigma_{min}, \sigma_{max}]$ , which implies  $\mathcal{M}(B) = 1$ ) or a sub-box resulting from the bisection satisfies property 2 or 3 which means that at some point in  $B$  at least one of the eigenvalues of  $\mathcal{P}$  lies outside the range  $[\sigma_{min}, \sigma_{max}]$ , which corresponds to  $\mathcal{M}(B) = 0$ .

The algorithm may indeed return 0 for a box that includes only valid points. But the width of this box will be lower than  $\alpha/2$  (where  $\alpha$  is an accuracy threshold fixed in advance for the computation) and hence the final result will be within the tolerance margin of the calculation. The only case in which the calculation will be not guaranteed will occur only when  $\alpha$  is lower than the machine accuracy. But we may determine that we are in such configuration as the width of the box from the machine viewpoint will be 0: if a box of width 0 is processed and the algorithm returns 0, then a warning message will be issued indicating that the calculation is no more guaranteed. Note, however, that we may still use the algorithm by using a multi-precision package such as MPFR that will allow to get a guaranteed result. Furthermore it is doubtful that computing the result with an accuracy better than the machine precision makes sense.

### 2.2.2 Invalid center point

Without lack of generality, we may assume that at the center of the box the largest eigenvalue is greater than  $\sigma_{max}$ . If there is no point in  $B$  such that one of the eigenvalues is equal to  $\sigma_{max}$ , then we can guarantee that for any point in  $B$  the largest eigenvalue is always greater than  $\sigma_{max}$  and consequently  $\mathcal{M}(B) = -1$ . This check is performed by using the same method as in the previous case.

## 2.3 A second basic tool: Box workspace verification

During the calculation of the dextrous workspace, we consider a Cartesian box  $B$  and we have to examine if this box may contain a point that is the center of a Cartesian box  $B_W$  with edge length  $w$ , which is fully enclosed in the robot workspace. We assume here that this workspace is defined by a set of  $m$  inequalities  $F_j$  such that a point  $X$  belongs to the workspace if  $F_j(X) \leq 0$  for all  $j$  in  $[1, m]$ . Let  $B_i$  be a sub-box included in  $B$ , defined by the three ranges  $[\underline{x}_i, \overline{x}_i]$ ,  $[\underline{y}_i, \overline{y}_i]$ ,  $[\underline{z}_i, \overline{z}_i]$ . All the boxes with edge length  $w$  that have as center a point in  $B_i$  are included in the *hull box*  $H_{B_i}$  defined by the three ranges  $[\underline{x}_i - w/2, \overline{x}_i + w/2]$ ,  $[\underline{y}_i - w/2, \overline{y}_i + w/2]$ ,  $[\underline{z}_i - w/2, \overline{z}_i + w/2]$ . As in the previous section we may use interval analysis to compute an interval evaluation  $[m_{B_i}^j, M_{B_i}^j]$  of all  $F_j(H_{B_i})$  with the following properties:

1. if  $M_{B_i}^j < 0$  for all  $j$  in  $[1, m]$ , then any point of  $B_i$  may be the center of a box with edge length  $w$  that is included in the workspace
2. if  $m_{B_i}^j > 0$ , then no point of  $B_i$  may be the center of a box with edge length  $w$  that is included in the workspace
3. if  $m_{B_i} < 0$  and  $M_{B_i} > 0$ , then we cannot determine if some point within  $B_i$  may be the center of  $B_W$

Note also that if the widths of all the ranges defining  $B_i$  are lower than  $w$ , any box  $B_W$  contains the 4 corners of the box  $B_i$ .

Using a similar branch-and-bound algorithm as in the previous section, we may now determine if either all, none or some points of  $B$  may be the center of a box  $B_W$ . The initial box  $B$  is bisected until either all the sub-boxes resulting from the bisection satisfy property 1 (then any point of  $B$  may be the center of a box  $B_W$ ), or 2 (no point of  $B$  may be the center of a box  $B_W$ ). If a sub-box satisfies property 3 and the widths of its ranges are lower than  $w$ , we check if the corners of  $B$  belong to the workspace: if all the corners either belong or do not belong to the workspace we continue the bisection. If we have a mixed situation with some corners belonging to the workspace whereas other ones do not, we may state that  $B$  contains both points that may be the center of a box  $B_W$  and points that cannot. A similar situation is obtained if we have found at least a sub-box that satisfies property 1 and a sub-box that satisfies property 2.

At that point we may define a procedure  $\mathcal{G}(B, w)$  that takes as input a box  $B$  and an edge length  $w$  and returns:

- -1: there is no points in  $B$  that may be the center of a box  $B_W$

- 1: all the points in  $B$  may be the center of a box  $B_W$
- 0:  $B$  contains both points that may be the center of a box  $B_W$  and points that cannot.

## 2.4 Algorithm for the determination of a cubic dextrous Cartesian workspace

An algorithm is now described for the determination of a cube that is enclosed in the Cartesian workspace and aligned with the coordinate axis, whose edge length is  $2w$  and such that there is no other cube enclosed in the workspace with an edge length of  $2(w + \alpha)$ . This algorithm can be applied to any 3-DOF manipulator. Other shapes for regular dextrous workspace is considered in section 2.5.

The first step is to determine the largest cube enclosed in the workspace with a center located at  $(0, 0, 0)$ . This is done by using the  $\mathcal{M}$  procedure on the Cartesian box  $B_{init} [-k\alpha, k\alpha], [-k\alpha, k\alpha], [-k\alpha, k\alpha]$  where  $k$  is an integer initialized to 1. Each time the  $\mathcal{M}$  procedure returns 1 for  $B_{init}$  (which means that the cube with edge length  $2k\alpha$  is enclosed in the dextrous workspace) we double the value of  $k$ . If this procedure returns -1 for a value of  $k$  larger than 1 this implies that the cube with edge length  $k\alpha/2$  is in the dextrous workspace whereas the cube with edge length  $k\alpha$  is not. Hence if  $k > 2$  (otherwise no improvement is possible) we restart the process with  $k = (k/2 + k)/2$ . After a failure at  $k_{fail}$  the principle is to always choose a value of  $k$  which is the mid-point between the last value  $k_s$  of  $k$  for which  $\mathcal{M} = 1$  and  $k_{fail}$  until  $k_{fail} = k_s + 1$ . For example if  $\mathcal{M}$  returns 1 for  $k=1, 2, 4$  and returns -1 for  $k = 8$  we set  $k$  to 6. Otherwise we have determined that the cube with edge length  $2k\alpha$  is enclosed in the dextrous workspace, whereas the cube with edge length  $2(k + 1)\alpha$  is not. The value  $2k\alpha$  is hence an initial value for  $w$ . Note that the above procedure may be used whatever the coordinates of the center: it is implemented as a general purpose procedure  $\mathcal{C}(x_M, y_M, z_M)$  that takes as input the coordinates of a point  $M$  and returns the edge length of the largest cube centered at  $M$ , that is enclosed in the dextrous workspace.

In the algorithm for determining the largest cube enclosed in the dextrous workspace, we manage a list of Cartesian boxes  $\mathcal{L}$  that are processed by the algorithm in sequence. During the processing, boxes may be added to a list. At one step of the algorithm we have  $n$  boxes in the list whereas processing box numbered  $i$  (which means that boxes numbered from 0 to  $i - 1$  have already been processed and may be discarded whereas boxes  $i$  to  $n$  have to be processed). The algorithm stops when all the boxes in  $\mathcal{L}$  have been processed. The box numbered  $i$  in the list is denoted  $B_i$  and the maximum number of boxes in  $\mathcal{L}$  is  $N$ .

At the beginning of the algorithm,  $\mathcal{L}$  has only one box  $B_0$  that contains the workspace (for example for the Orthoglide  $B_0 = \{[-L, L], [-L, L], [-L, L]\}$ ). The algorithm can be described by the following six steps:

1. calculate  $w = C(0, 0, 0)$
2. if  $i > n$  EXIT
3. if  $\mathcal{G}(B_i, w + \alpha) = -1$ , then set  $i$  to  $i + 1$  and go to 2

4. if  $\mathcal{G}(B_i, w + \text{alpha}) = 1$ , then calculate  $w' = C(x_{B_i}, y_{B_i}, z_{B_i})$  where  $x_{B_i}, y_{B_i}, z_{B_i}$  are the coordinates of the center of  $B_i$ . If  $w' > w$ , then update  $w$ . Go to step 6
5. if  $\mathcal{G}(B_i, w + \text{alpha}) = 0$ , then go to step 6
6. bisect the variable in the box  $B_i$  that has the largest range. For example if the box  $B_i$  is defined as  $[\underline{x}_i, \overline{x}_i], [\underline{y}_i, \overline{y}_i], [\underline{z}_i, \overline{z}_i]$  and the variable  $x$  has the largest range the bisection process creates two new boxes  $B_i^1 = \{[\underline{x}_i, (\underline{x}_i + \overline{x}_i)/2], [\underline{y}_i, \overline{y}_i], [\underline{z}_i, \overline{z}_i]\}$  and  $B_i^2 = \{[(\underline{x}_i + \overline{x}_i)/2, \overline{x}_i], [\underline{y}_i, \overline{y}_i], [\underline{z}_i, \overline{z}_i]\}$ . If  $n < N/2$ , both boxes are stored at the end of the list (and we set  $i=i+1$ ), otherwise Box  $B_i^1$  are stored in  $\mathcal{L}$  in place of  $B_i$  whereas box  $B_i^2$  is stored at location  $i + 1$  after a shift of the boxes  $B_{i+1}, \dots, B_n$ . Set  $n$  to  $n + 1$  and go to 2.

Step 1 allows one to establish an initial value for the maximal edge length. Step 3 eliminates boxes that cannot contain the center of the maximal cube due to the workspace limits. Boxes satisfying step 4 are candidate to include the center of the largest cube: hence we calculate the largest cube centered at the box that may allow to update the current value of the largest edge. Step 6 is the bisection process that allows one to decrease the size of the box with the effect of a sharper calculation for the procedure  $\mathcal{G}$ . Note also that two storage modes that are used for adding the boxes resulting from the bisection process. The second mode allows for a minimal memory storage but has the drawback of focusing on a given part of the workspace whereas the center of the largest cube may be located in another part. The first mode makes it possible to explore various parts of the workspace which may result in large improvement on the value of  $w$  but as the drawback of possibly creating a large number of boxes. The proposed storage mode allows one to mix the advantages of both storage modes.

This procedure ensures to determine a cube with edge length  $w$  that is enclosed in the workspace and in the dextrous workspace, whereas there is no such cube with edge length  $w + \alpha$ .

Note that an incremental approach is possible. After having computed  $w = w_1$  with a given accuracy  $\alpha$  it is always possible to replace the initial value of  $w$  as calculated in step 1 of the algorithm by the value  $w_1$  when computing the cube with a lower value for  $\alpha$ . Computation times of the largest cube for various accuracies are given for a specific 3-DOF PKM in section 4.3.

## 2.5 Other regular dextrous workspace shapes

Clearly, considering the largest cube may not be appropriate if the studied PKM has a rectangular or a spherical-shaped workspace. The algorithm can thus be modified. Here are for example the necessary changes that must be taken into account to consider the largest sphere: the idea is to use spherical coordinates and hence  $x, y, z$  are substituted by  $x_c + r \sin \psi \sin \theta, y_c + r \cos \psi \sin \theta, z_c + r \cos \theta$ , with  $r$  in  $[0, R]$ ,  $\psi, \theta$  in  $[0, 2\pi]$ ,  $x_c, y_c, z_c$  being the coordinates of the center of the sphere and  $R$  its radius. Interval analysis allows to deal with expressions involving sine and cosine and hence procedures  $\mathcal{M}, \mathcal{G}$  can still be used with these new parameters. Similarly procedure  $\mathcal{C}(x_M, y_M, z_M)$  can be used to determine the largest radius of the sphere centered at  $(x_M, y_M, z_M)$  for

which the eigenvalues are valid. Hence, with this modification, the algorithm can calculate the largest sphere enclosed in the dextrous workspace.

Spheres and cubes are defined by their center and one additional parameter. But other shapes may involve more parameters: for example a cylinder needs a center but also a height and a radius. We can still perform a change in the variables so that procedures  $\mathcal{M}, \mathcal{G}$  can still be used. The key point is that procedure  $\mathcal{C}(x_M, y_M, z_M)$  has to be modified as we have now two optimization parameters. But in that case volume optimization alone has less meaning: for example the optimization result for a cylinder may be a cylinder with a relatively small radius and a large height, which may be of no interest. A cylinder of identical radius and height with a lower volume may be the most interesting result. A possible way to manage this problem is to assign a range  $[a, b]$  for the ratio  $R/h$  where  $R$  is the cylinder radius and  $h$  its height. In that case the procedure  $\mathcal{C}$  has to solve an optimization problem which is to maximize the volume of the cylinder under the constraints that the eigenvalues are valid and the ratio  $R/h$  satisfies  $a \leq R/h \leq b$ . ALIAS is still able to manage such an optimization procedure.

## 2.6 Approximate calculation of the dextrous workspace

Small modifications in the previous algorithm allow to determine an approximation of the dextrous Cartesian workspace  $\mathcal{W}_{Dextrous}$  as a set  $\mathcal{S}$  of 3D Cartesian boxes such that for any box  $B$  in  $\mathcal{S}$  and for any point in  $B$  the constraints on the eigenvalues are satisfied. The width of all the boxes in the set  $\mathcal{S}$  is greater than a given threshold  $\epsilon$ : hence we get only an approximation of the dextrous Cartesian workspace. But the algorithm provides the volume  $V_a$  of the approximation and a volume error  $V_e$  such that the volume  $V_d$  of the dextrous Cartesian workspace satisfies  $V_d \leq V_a + V_e$ . Decreasing the value of  $\epsilon$  makes it possible to increase  $V_a$  and to decrease  $V_e$ . In this paper, this method is used to analyze 3D boxes but it can be applied for any mechanism with  $n$  d.o.f., the result being a set of  $n$ D boxes.

Initially  $V_a, V_e$  are set to 0.

1. if  $i > n$  EXIT
2. if  $\mathcal{M}(B_i) = -1$ , then set  $i$  to  $i + 1$  and go to 1
3. if  $\mathcal{M}(B_i) = 1$ , then store  $B_i$  in  $\mathcal{S}$  and add its volume to  $V_a$ . Set  $i$  to  $i + 1$  and go to 1
4. if  $\mathcal{M}(B_i) = 0$ , then
  - (a) if the largest width of  $B_i$  is lower than  $\epsilon$ , then add its volume to  $V_e$ , set  $i$  to  $i + 1$  and go to 1
  - (b) otherwise go to step 5
5. process bisection for the box  $B_i$ . Set  $n$  to  $n + 1$  and go to 1

Note that this procedure may be incremental if the boxes neglected at step 4-a are stored in a file  $\mathcal{F}$ . Indeed a first run with a given  $\epsilon$  allows to obtain initial values for  $V_a, V_e$ . If the quality of the approximation is not satisfactory, we may choose a smaller value of  $\epsilon$  (e.g.  $\epsilon/2$ ). But instead of starting with the initial  $B_0$ , we may

use the boxes stored in  $\mathcal{F}$ , thereby avoiding to repeat computation that has already been done during the initial run.

### 3 Description of the Orthoglide and the UraneSX

The previous interval analysis based design method is now applied to the comparison of two 3-DOF translational PKM. It is particularly interesting to compare these two mechanisms because they belong to the same architecture family.

#### 3.1 Orthoglide and UraneSX architectures

Most existing PKM can be classified into two main families. PKM of the first family have fixed foot points and variable length struts and are generally called “hexapods” or “tripods”. PKM of the second family have variable foot points and fixed length struts. They are interesting because the actuators are fixed and thus the moving masses are lower than in the hexapods and tripods.

The Orthoglide and the UraneSX mechanisms studied in this paper are 3-DOF translational PKM and belong to the second family. Figures 1 and 2 show the general kinematic architecture of the Orthoglide and of the UraneSX, respectively. Both mechanisms have three parallel  $PRPaR$  identical chains (where  $P$ ,  $R$  and  $Pa$  stand for Prismatic, Revolute and Parallelogram joint, respectively). The actuated joints are the three linear joints. These joints can be actuated by means of linear motors or by conventional rotary motors with ball screws.

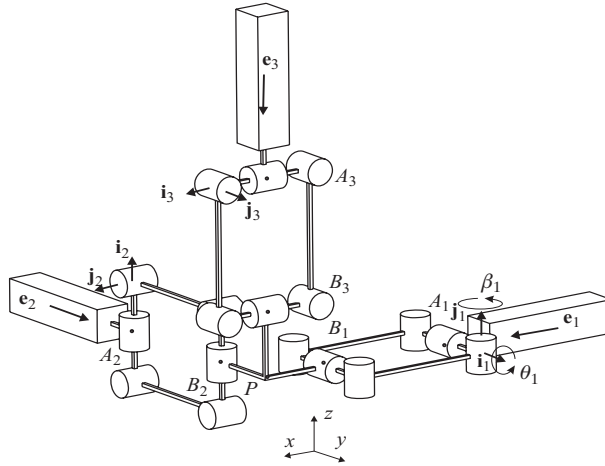


Figure 1: Orthoglide kinematic architecture

The output body is connected to the linear joints through a set of three parallelograms of equal lengths  $L = A_i B_i$ , so that it can move only in translation. Vectors  $e_i$  coincide with the direction of the  $i^{th}$  linear joint. The base points  $A_i$  are located at the middle of the first two revolute joints of the  $i^{th}$  parallelogram, and  $B_i$  is at the middle of the last two revolute joints of the  $i^{th}$  parallelogram.

For the Orthoglide mechanism, the first linear joint axis is parallel to the  $x$ -axis, the second one is parallel to the  $y$ -axis and the third one is parallel to the  $z$ -axis. When each vector  $\mathbf{e}_i$  is aligned with  $\mathbf{A}_i\mathbf{B}_i$ , the Orthoglide is in an isotropic configuration and the tool center point  $P$  is located at the intersection of the three linear joint axes.

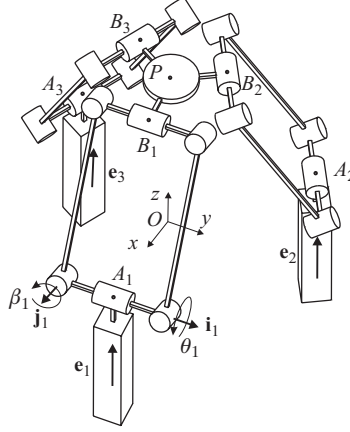


Figure 2: UранеSX kinematic architecture

The linear joint axes of the UранеSX mechanism are parallel to the  $z$ -axis. In fig. 2, points  $A_1$ ,  $A_2$  and  $A_3$  are the vertices of an equilateral triangle whose geometric center is  $O$  and such that  $OA_i = R$ . Thus, points  $B_1$ ,  $B_2$  and  $B_3$  are the vertices of an equilateral triangle whose geometric center is  $P$ , and such that  $OB_i = r$ .

### 3.2 Kinematic equations and singularity analysis

We recall briefly here the kinematic equations and the singularities of the Orthoglide and of the UранеSX (See [20, 19] for more details).

Let  $\theta_i$  and  $\beta_i$  denote the joint angles of the parallelogram about axes  $\mathbf{i}_i$  and  $\mathbf{j}_i$ , respectively (Figs. 1 and 2). Let  $\rho_1, \rho_2, \rho_3$  denote the linear joint variables and  $L$  denote the length of the three legs,  $A_iB_i$ .

For the Orthoglide, the position vector  $\mathbf{p}$  of the tool center point  $P$  is defined in a reference frame  $(O, x, y, z)$  centered at the intersection of the three linear joint axes (note that the reference frame has been translated in Fig. 1 for more legibility).

For the UранеSX, the position vector  $\mathbf{p}$  of the tool center point  $P$  is defined in a reference frame  $(O, x, y, z)$  centered at the geometric center of the points  $A_1, A_2$ , and  $A_3$  (same remark as above).

Let  $\dot{\boldsymbol{\rho}}$  be referred to as the vector of actuated joint rates and  $\dot{\mathbf{p}}$  as the velocity vector of point  $P$ :

$$\dot{\boldsymbol{\rho}} = [\dot{\rho}_1 \ \dot{\rho}_2 \ \dot{\rho}_3]^T, \quad \dot{\mathbf{p}} = [\dot{x} \ \dot{y} \ \dot{z}]^T \quad (2)$$

$\dot{\mathbf{p}}$  can be written in three different ways by traversing the three chains  $A_iB_iP$ :

$$\dot{\mathbf{p}} = \mathbf{e}_i\dot{\rho}_i + (\dot{\theta}_i\mathbf{i}_i + \dot{\beta}_i\mathbf{j}_i) \times (\mathbf{b}_i - \mathbf{a}_i) \quad (3)$$

where  $\mathbf{a}_i$  and  $\mathbf{b}_i$  are the position vectors of the points  $A_i$  and  $B_i$ , respectively, and  $\mathbf{e}_i$  is the direction vector of the linear joints, for  $i = 1, 2, 3$ .

We want to eliminate the three idle joint rates  $\dot{\theta}_i$  and  $\dot{\beta}_i$  from Eqs. (3), which we do by dot-product of Eqs. (3) by  $\mathbf{b}_i - \mathbf{a}_i$ :

$$(\mathbf{b}_i - \mathbf{a}_i)^T \dot{\mathbf{p}} = (\mathbf{b}_i - \mathbf{a}_i)^T \mathbf{e}_i \dot{\rho}_i \quad (4)$$

Equations (4) can now be cast in vector form, namely  $\mathbf{A}\dot{\mathbf{p}} = \mathbf{B}\dot{\boldsymbol{\rho}}$ , where  $\mathbf{A}$  and  $\mathbf{B}$  are the parallel and serial Jacobian matrices, respectively:

$$\mathbf{A} = \begin{bmatrix} (\mathbf{b}_1 - \mathbf{a}_1)^T \\ (\mathbf{b}_2 - \mathbf{a}_2)^T \\ (\mathbf{b}_3 - \mathbf{a}_3)^T \end{bmatrix} \quad \text{and} \quad \mathbf{B} = \begin{bmatrix} \eta_1 & 0 & 0 \\ 0 & \eta_2 & 0 \\ 0 & 0 & \eta_3 \end{bmatrix} \quad (5)$$

with  $\eta_i = (\mathbf{b}_i - \mathbf{a}_i)^T \mathbf{e}_i$  for  $i = 1, 2, 3$ .

Parallel singularities occur when the determinant of the matrix  $\mathbf{A}$  vanishes, *i.e.* when  $\det(\mathbf{A}) = 0$ . Eq. (5) shows that the parallel singularities occur when:

$$(\mathbf{b}_1 - \mathbf{a}_1) = \alpha(\mathbf{b}_2 - \mathbf{a}_2) + \lambda(\mathbf{b}_3 - \mathbf{a}_3) \quad (6)$$

that is when the points  $A_1, B_1, A_2, B_2, A_3$  and  $B_3$  lie in parallel planes. A particular case occurs when the links  $A_i B_i$  are parallel:

$$\begin{aligned} (\mathbf{b}_1 - \mathbf{a}_1) & \parallel (\mathbf{b}_2 - \mathbf{a}_2) \quad \text{and} \\ (\mathbf{b}_2 - \mathbf{a}_2) & \parallel (\mathbf{b}_3 - \mathbf{a}_3) \quad \text{and} \\ (\mathbf{b}_3 - \mathbf{a}_3) & \parallel (\mathbf{b}_1 - \mathbf{a}_1) \end{aligned}$$

Serial singularities arise when the serial Jacobian matrix  $\mathbf{B}$  is no longer invertible *i.e.* when  $\det(\mathbf{B}) = 0$ . At a serial singularity a direction exists along which no Cartesian velocity can be produced. Equation (5) shows that  $\det(\mathbf{B}) = 0$  when for one leg  $i$ ,  $(\mathbf{b}_i - \mathbf{a}_i) \perp \mathbf{e}_i$ .

When  $\mathbf{B}$  is not singular, we can write,

$$\dot{\boldsymbol{\rho}} = \mathbf{J}^{-1} \dot{\mathbf{p}} \quad \text{with} \quad \mathbf{J}^{-1} = \mathbf{B}^{-1} \mathbf{A} \quad (7)$$

## 4 Comparison of the Orthoglide and the UraneSX

In this section, we calculate the edge length of the largest cube for the Orthoglide, the edge length of the largest square for the UraneSX, as well as the location of their respective centers. To simplify the problem, the bounds

on the velocity transmission factors are such that  $\psi_{min} = 1/\psi_{max}$ .

#### 4.1 Regular dextrous workspace shape

The Orthoglide and the UraneSX are compared according to the size of their largest regular dextrous Workspace. Due to the symmetrical architecture of the Orthoglide, the Cartesian workspace has a fairly regular shape in which it is possible to include a cube whose sides are parallel to the planes  $xy$ ,  $yz$  and  $xz$  respectively. The Cartesian workspace of the UraneSX is the intersection of three cylinders whose axes are parallel to the  $z$ -axis. Thus, the workspace is unlimited in the  $z$ -direction and the Jacobian matrix does not depend on the  $z$  coordinate. Only the limits on the linear joints define the limits of the Cartesian workspace in the  $z$ -direction. However, it is possible to include a square in the plane  $xy$ . Regular dextrous workspaces are thus chosen to be a cube for the Orthoglide and a square for the UraneSX.

#### 4.2 Geometric constraints

Section 2.1 is suggested to add geometrical constraints so as to decrease the computing time and to avoid numerical problems on singularities. Here, polynomial  $\mathcal{P}$  is defined only for the points within the intersection  $\mathcal{I}$  of the three cylinders defined by

$$x^2 + y^2 < L^2 \quad x^2 + z^2 < L^2 \quad y^2 + z^2 < L^2 \quad (8)$$

for the Orthoglide, and,

$$\begin{aligned} (x - R + r)^2 + y^2 &< L^2 \\ \left(x - (R - r)\frac{1}{2}\right)^2 + \left(y - (R - r)\frac{\sqrt{3}}{2}\right)^2 &< L^2 \\ \left(x - (R - r)\frac{1}{2}\right)^2 + \left(y + (R - r)\frac{\sqrt{3}}{2}\right)^2 &< L^2 \end{aligned}$$

for the UraneSX. With these constraints, matrix  $\mathbf{B}$  is never singular and thus can be always inverted. To solve numerically the above equations and to compare the two mechanisms, the length of the legs is normalized, *i.e.* we set  $L = 1$ .

#### 4.3 Comparison results

To compare the two mechanisms studied, the leg length  $L$  is set to 1 and the bounds on the velocity factor amplification are set to  $\psi = [0.5 \ 2]$ , with  $\alpha = 0.001$ . For the UraneSX, it is necessary to define two additional lengths,  $r$  and  $R$ . However, the edge length of the workspace depends only on  $R - r$ .

For the Orthoglide, it is found that the largest cube has its center located at  $(0.086, 0.086, 0.086)$ , and that the cube edge length is  $L_{Workspace} = 0.644$ . Also, using the incremental approach described in section 2.4, we

get for the Orthoglide the computation time of Table 1 on a Sun Blade workstation.

Accuracy $\alpha$ (mm)	0.01	0.001	0.0001	0.00001
Computation time (s)	360	150	504	900

Table 1: **Computation time of the largest cube enclosed in the dextrous workspace for various accuracies**

For the UraneSX, the design parameters are those defined in [20], which we have normalized to have  $L = 1$ , *i.e.*  $r = 3/26$  and  $R = 7/13$ . To compare the two mechanisms, we increase the value of  $R$  such that  $R' = R + \lambda$  with  $\lambda = [0.0, 0.2]$ . For  $R < 7/13$ , the constraints on the velocity amplification factors are not satisfied.

$\lambda$	Center	$L_{Workspace}$
0.00	(-0.0178,-0.0045)	0.510
0.05	(-0.0179,-0.0022)	0.470
0.10	(-0.0225,-0.0031)	0.420
0.15	(-0.0245,-0.0018)	0.370
0.20	(-0.0211,-0.0033)	0.320

Table 2: **Variations of the edge length of the square workspace for the UraneSX mechanism**

The optimal value of  $R'$  is obtained for  $\lambda = 0$ , *i.e.* for the design parameters defined in [20] for an industrial application (see table 2). To expand this square workspace in the  $z$ -direction, the range limits must be equal to the edge length of the square plus the range variations necessary to move throughout the square in the  $x - y$  plane.

The constraints on the velocity amplification factors used for the design of the Orthoglide are close to those used for the design of the UraneSX which is an industrial machine tool. For the same length of the legs, the size of the cubic workspace is larger for the Orthoglide than for the UraneSX.

For the Orthoglide, the optimization puts the serial and parallel singularities far away from the Cartesian workspace [19]. The UraneSX has no parallel singularities due to the design parameters ( $R - r < L$ ), but serial singularities cannot be avoided with the previous optimization function. To produce the motion in the  $z$ -direction, the range limits of the linear joints are set such that the constraints on the velocity amplification factors are not satisfied throughout the Cartesian workspace.

The range limits  $\Delta\rho_i$  of each prismatic joint can be decomposed into two parts. For the Orthoglide (resp. for the UraneSX), the first part  $\Delta f_i$  makes it possible to move the mobile platform throughout the face of the prescribed cube that is perpendicular to the considered prismatic joint axis (resp. throughout the prescribed square). The second part is equal to the edge length of the cubic workspace  $L_{Workspace}$ . The equations of the inverse kinematic model allow us to compute  $\Delta f_i$  for the two mechanisms.

For the Orthoglide, the position and the size of the prescribed cube define three range limits for the  $x - y - z$  platform coordinates,

$$x = [-0.322 + 0.085, 0.322 + 0.085] \quad (9a)$$

$$y = [-0.322 + 0.085, 0.322 + 0.085] \quad (9b)$$

$$z = [-0.322 + 0.085, 0.322 + 0.085], \quad (9c)$$

For the UraneSX, the position and the size of the prescribed square define two range limits for the  $x - y$  platform coordinates,

$$x = [-0.255 - 0.018, 0.255 - 0.018] \quad (9d)$$

$$y = [-0.255, 0.255]. \quad (9e)$$

For the Orthoglide, all  $\Delta f_i$  are equal due to the symmetrical architecture. For the UraneSX, we take  $\Delta f = \text{Max}(\Delta f_i)$ . The results are  $\Delta f = 0.181$  and  $\Delta \rho = 0.825$  for the Orthoglide and  $\Delta f = 0.353$  and  $\Delta \rho = 0.863$  for the UraneSX. This means that the range limits are quite similar for the same leg length. To calculate the volume of the Cartesian workspace of the two mechanisms for the previous range limits, we have used a CAD system. Results are given in table 3.

	Cartesian workspace volume with optimized ranges limits	cubic dextrous workspace volume	ratio
Orthoglide	0.566	0.265	46.8%
UraneSX	0.544	0.132	24.3%

Table 3: **Workspace volumes of the two mechanisms**

To help understand these results, Fig. 3 and 4 show the location of the largest cubic workspace inside the Cartesian workspace. As the Cartesian workspace of the Orthoglide is regular and admits a quasi-cubic shape, the ratio between the cubic workspace and the Cartesian workspace is better than for the UraneSX.

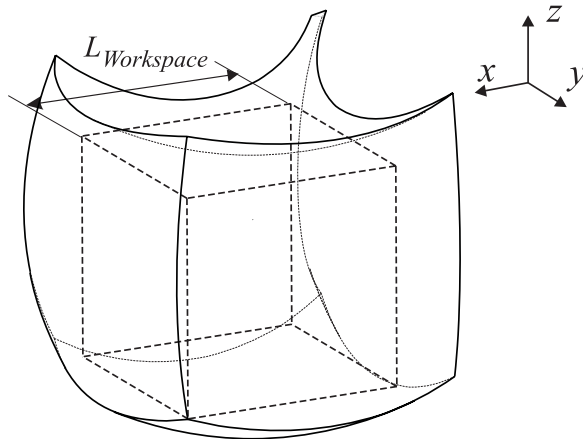


Figure 3: **Cartesian workspace and dextrous workspace for the Orthoglide mechanism with optimized range limits**

In table 4, the design parameters are compared to achieve the same cubic dextrous workspace with  $L_{Workspace} = 1$ . The legs length is directly connected to the dynamic properties of the mechanism. The range limits and the

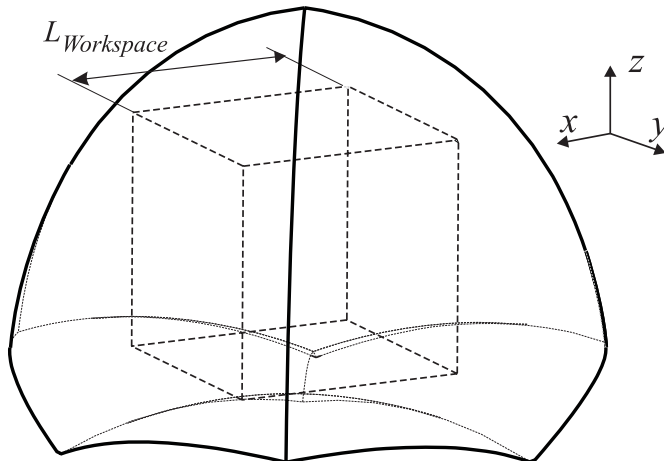


Figure 4: Cartesian workspace and dextrous workspace for the UraneSX mechanism with optimized range limits

legs length are important parameters in the determination of the total size of the mechanism and in its global cost. The volume of the Cartesian workspace allows us to characterize the shape and the volume of motion of the tool with regard to the useful Cartesian workspace dedicated to manufacturing tasks (cubic workspace).

	Leg length	Range limits	Volume of the Cartesian workspace
Orthoglide	1.55	1.28	2.13
UraneSX	1.96	1.69	4.12

Table 4: Synthesis of the comparative study for the same cubic Cartesian workspace

These criteria allow us to optimize some geometric parameters to design a machine tool for milling applications. Although in this approach, the kinetostatic properties of the Orthoglide are better than the UraneSX ones, we cannot assert that the Orthoglide is better than the UraneSX. One reason is that these two PKM are not aimed at identical manufacturing tasks. The main applications of the UraneSX are drilling, facing and tapping whereas the Orthoglide is more universal.

Other shapes of regular dextrous workspaces can be computed for the Orthoglide and the UraneSX by using cylindrical or spherical coordinates to have the largest cylinder or sphere respectively, even if these shapes are generally less relevant for milling applications.

## 5 Conclusions

This paper introduces an interval analysis based study for the design and the comparison of 3-DOF PKM. Two basic tools and an algorithm are described to determine the largest regular dextrous workspace enclosed in the Cartesian workspace. The dextrous workspace is a part of the Cartesian workspace in which the velocity amplification factors remain within a predefined range. This means that throughout the dextrous workspace, milling tool paths are available because the variations of the kinematic performances index remain under reasonable

values. The regular dextrous workspace shape is a cube for the Orthoglide and a square for the UraneSX. This general method is coupled with geometric constraints associated with the mechanisms studied to avoid numerical problems at singular configurations. The shape of the dextrous workspace was chosen for milling applications but it can be different for other applications. The range limits and the volume of the Cartesian workspace were calculated to compare the two mechanisms.

## 6 Acknowledgments

This research was supported by the CNRS (Project ROBEA “Machine Architecture complexe”). We would like to thank the anonymous reviewers for their very useful comments.

## References

- [1] Merlet, J-P., 1996, “Workspace-Oriented Methodology for Designing a Parallel Manipulator,” IEEE Int. Conf. on Robotics and Automation, pp. 3726–3731.
- [2] Clavel, R., 1988, “DELTA, a Fast Robot with Parallel Geometry,” Proc. of the 18th Int. Symposium of Industrial Robots, IFR Publications, pp. 91–100.
- [3] Gosselin, C and Angeles, J., 1991, “A Global Performance Index for the Kinematic Optimization of Robotic Manipulators,” Journal of Mechanical Design, vol. 113, pp. 220–226.
- [4] Wenger, Ph. and Chablat, D., 1997, “Definition Sets for the Direct Kinematics of Parallel Manipulators,” 8th Int. Conf. Advanced Robotics, pp. 859–864.
- [5] Kim, J. Park, C. Kim, J. and Park, F.C. 1997, “Performance Analysis of Parallel Manipulator Architectures for CNC Machining Applications,” Proc. IMECE Symp. On Machine Tools, Dallas.
- [6] Treib, T. and Zirn, O. 1998, “Similarity laws of serial and parallel manipulators for machine tools,” Proc. Int. Seminar on Improving Machine Tool Performance, Vol. 1, pp. 125–131.
- [7] Wenger, P. Gosselin, C. and Chablat, D. 2001, “A Comparative Study of Parallel Kinematic Architectures for Machining Applications,” Proc. Workshop on Computational Kinematics’2001, Seoul, Korea, pp. 249–258.
- [8] Kong, X. and Gosselin, C. M., 2002, “A Class of 3-DOF Translational Parallel Manipulators with Linear I-O Equations,” Proc. of Workshop on Fundamental Issues and Future Research Directions for Parallel Mechanisms and Manipulators, Québec, Canada, CD-ROM.
- [9] Carricato, M. and Parenti-Castelli, V., 2002, “Singularity-Free Fully-Isotropic Translational Parallel Mechanisms,” The Int. Journal of Robotics Research, Vol. 21, No. 2, pp. 161-174, February.

- [10] Rehsteiner, F., Neugebauer, R., Spiewak, S. and Wieland, F., 1999, "Putting Parallel Kinematics Machines (PKM) to Productive Work," *Annals of the CIRP*, Vol. 48:1, pp. 345–350.
- [11] Tlustý, J., Ziegert, J. and Ridgeway, S., 1999, "Fundamental Comparison of the Use of Serial and Parallel Kinematics for Machine Tools," *Annals of the CIRP*, Vol. 48:1, pp. 351–356.
- [12] Luh C-M., Adkins F. A., Haug E. J. and Qui C. C., 1996, "Working Capability Analysis of Stewart platforms," *Transactions of ASME*, pp. 220–227.
- [13] Merlet J-P., 1999, "Determination of 6D Workspace of Gough-Type Parallel Manipulator and Comparison between Different Geometries," *The Int. Journal of Robotic Research*, Vol. 19, No. 9, pp. 902–916.
- [14] Stoughton, R. S. and Arai T., 1993, "A modified Stewart Platform Manipulator with Improved Dexterity," *IEEE Transactions On Robotics and Automation*, April, Vol. 9, No. 2, pp. 166–173.
- [15] Gosselin, C., and Angeles, J., 1988, "The Optimum Kinematic Design of a Planar Three-Degree-of-Freedom Parallel Manipulator," *ASME, Journal of Mechanisms, Transmissions, and Automation in Design*, March, Vol. 110.
- [16] Merlet, J-P., 2000, "ALIAS: an interval analysis based library for solving and analyzing system of equations," *SEA, June. Automation*, pp. 1964–1969.
- [17] Chablat, D., Wenger, Ph. and Merlet J-P, 2002, "Workspace Analysis of the Orthoglide using Interval Analysis," *8th International Symposium on Advances in Robot Kinematics*, Kluwer Academic Publishers, Caldes de Malavella, Spain, June, pp. 397–406.
- [18] Joshi, S. and Tsai, L.W., 2003, "A Comparison Study of Two 3-DOF Parallel Manipulators: One with Three and the other with Four Supporting Legs," *IEEE Transactions On Robotics and Automation*, April, Vol. 19, No. 2, pp. 200–209.
- [19] Chablat, D. and Wenger, Ph, 2003, "Architecture Optimization of a 3-DOF Parallel Mechanism for Machining Applications, the Orthoglide," *IEEE Transactions On Robotics and Automation*, June, Vol. 19, No 3, pp. 403–410.
- [20] Company, O. and Pierrot, F., 2002, "Modelling and Design Issues of a 3-axis Parallel Machine-Tool," *Mechanism and Machine Theory*, Vol. 37, pp. 1325–1345.
- [21] Moore, R.E., 1979, "Methods and Applications of Interval Analysis," *SIAM Studies in Applied Mathematics*, Philadelphia.
- [22] Neumaier, A., 1990, "Interval methods for systems of equations," *Cambridge University Press*, Cambridge.
- [23] Ratscheck, H. and Rokne, J., 1995, "Interval methods," *Handbook of global optimization*, Kluwer, Horst, R. and Pardalos, P.M. Editors, pp. 751–819.